Comprehensive characterization of Al-doped ZnO thin films deposited in confocal radio frequency magnetron co-sputtering

Fatiha Challali, Tahar Touam, Valérie Bockelée, Thierry Chauveau, Azeddine Chelouche, Nicolas Stephant, Jonathan Hamon, Marie-Paule Besland

Comprehensive characterization of Al-doped ZnO thin films deposited in confocal radio frequency magnetron co-sputtering

Fatiha Challali[a*], Tahar Touam[b], Valérie Bockelée[a], Thierry Chauveau[a], Azeddine Chelouche[c], Nicolas Stephant[d], Jonathan Hamon[d], Marie-Paule Besland[d]

[a] *Laboratoire des Sciences des Procédés et des Matériaux, UPR CNRS 3407, Université Sorbonne Paris Nord, France*
[b]*Laboratoire des Semi-conducteurs, Université Badji Mokhtar-Annaba, 23000 Annaba, Algeria*
[c]*Laboratoire de Génie de l'Environnement, Université de Bejaia, 06000 Bejaïa, Algeria*
[d] *Nantes Université, CNRS, Institut des Matériaux de Nantes Jean Rouxel, IMN, F-44000 Nantes, France*

* *Corresponding author: fatiha.challali@univ-paris13.fr*

Abstract

Al-doped ZnO thin films with varying Aluminium (Al) content were deposited by radio frequency magnetron co-sputtering of two ZnO and Al targets in confocal configuration. A comprehensive study of the effect of Al content variation on the structural, optical and electrical properties were studied for as-deposited films and after an annealing step under controlled argon atmosphere. Chemical composition analyses, performed by both X-ray photoelectron spectroscopy and energy dispersive X-ray spectrometry, show an Al content variation in the deposited films in the 0-14 at.% range by varying the Al target power from 0 to 30 W, while the Zn target power was kept constant at 200 W. All deposited films exhibit a wurtzite crystalline structure and a decreasing crystalline quality for Al content above 5 at.% as shown by grazing incidence X-ray diffraction patterns. Atomic Force Microscopy analysis revealed films with homogeneous and dense surface morphology with roughness in the one nm range. Carrier concentration, resistivity and photoluminescence vary significantly with Al content in the ZnO films and appear optimized for an Al content window ranging from 1.5 to 5.5 at. %. Both optical and electrical properties are improved by a post-annealing at 300 °C under argon. A high figure of merit of 43.6×10^{-4} sq.Ω^{-1} was obtained for the ZnO film with Al content of 3.6 at.% after annealing at 300 °C. Optimized

properties are obtained for a higher Al content than the standard value of 2 at. % widely used in published works.

Keywords: Zinc oxide; Thin film; Aluminum content; Magnetron Sputtering; Optical and electrical characterizations

1. Introduction

Zinc oxide (ZnO) thin films are receiving a renewed interest due to their excellent electrical and optical properties as well as their wide bandgap, abundance and non-toxicity [1, 2]. The optoelectronic properties of ZnO thin films are related to the non-stoichiometry of the films, leading to the presence of oxygen vacancies and interstitial zinc within the crystalline network [3, 4]. The electrical behavior of ZnO films could be improved by replacing Zn^{2+} species with impurity dopants that have higher valences within Group III elements, such as In^{3+}, Al^{3+} or Ga^{3+} [5–10]. Al and Ga are reported as the best dopants to achieve transparent and conductive ZnO films [11, 12]. Indeed, Al-doped ZnO (AZO) thin films exhibit suitable properties as a transparent conductive oxide (TCO) with a high transparency of almost 90% in the visible spectral region and a covalent bond length of Al–O (192 pm) close that the one of Zn–O (197 pm). However, due to the large ionic radius mismatch and charge imbalance between aluminum ions (Al^{3+}) and Zinc ions (Zn^{2+}), the incorporation of aluminum into the ZnO lattice has always been quite a challenge [13, 14]. Moreover, physicochemical and optoelectronic properties generally depend on the deposition and post-deposition conditions. These properties can be significantly altered by the absorption or desorption of oxygen generated at different steps in the process [15–17].

ZnO can be obtained in thin films at relatively low deposition temperature with good stability using different methods, namely metal-organic chemical vapor deposition [18,

19], plasma-enhanced atomic layer deposition [20], sol-gel methods [21, 22], spray pyrolysis [23, 24], pulsed laser deposition [25] and sputtering [26].

In literature, Al doped ZnO sputtered thin films have been prepared via several approaches: (i) a doped ZnO target with a fixed Al_2O_3 or Al content (2 wt.%) [27-30], (ii) a ZnO target with Al metal inserts on the surface [31] and iii) a metallic Zn-Al alloy target with a fixed Al content in reactive mode [32,33]. A last approach to obtain Al-doped ZnO films is the co-sputtering of two targets, such as ZnO and Al_2O_3 [34-35], AZO and Zn [36], ZnO and Al [37, 38] or pure metallic targets Zn and Al in Ar/O_2 reactive atmosphere [39-41]. Nevertheless, several drawbacks are encountered in such configurations: quite low deposition rate, Al/Zn ratio arbitrarily fixed around 2 wt.%. Hence, controlling th concentration and the homogeneity of the dopant is often a great challenge. Moreover, in the case of metallic target, the metallic dopant may segregate in the grain boundaries or produce another phases. In all cases, the main challenge for sputtered AZO thin films is to achieve a homogeneous, uniform chemical composition and uniform thickness over a large area, which is required for industrial applications to reduce film production costs and spatial inhomogeneity of resistivity. For example Stamate [42] and Norrman et al. [43] reported the best range of sputtering parameters and demonstrated the importance of spatially distributed profiles for the optoelectronic properties of AZO thin films that can be used by conventional magnetron sputtering of a sintered single AZO target.

Despite the numerous studies carried out on the Al doped ZnO thin films, it appears that optimization of the free carriers concentration remains a challenge. Very few works have been reported on the effect of Al content variation in a large range into the ZnO films. Indeed, above a certain concentration limit, the microstructure and optoelectronic properties of the deposited films can be damaged by ionized impurities diffusion [44]. Moreover, very rare investigations have been published on the optimization of AZO films

obtained by confocal co-sputtering, where the target is positioned at an angle with respect to the surface of the substrate [45, 46]. Confocal magnetron co-sputtering, in combination with substrate rotation around its own axis, enables the deposition of multiple materials without breaking the chamber vacuum. This experimental setup allows obtaining good deposition rates, uniform film thickness and homogeneous material flexibility over an area larger than the size of the target. Hence, our aim is to use the confocal deposition of AZO films from two targets ZnO and Al in a non-reactive atmosphere to achieve good quality thin films with a high degree of uniformity and homogeneous material over large area substrates. The results were compared to those recently obtained on films deposited from a single AZO target in the same chamber [47].

In this work, we performed a comprehensive study of the effect of Al atoms incorporation into the ZnO matrix on the films properties. The aim of our study is to determine if the film characteristics can be improved by co-sputtering in confocal configuration. Al-doped ZnO films were prepared by non-reactive magnetron co-sputtering from two targets (ZnO and Al) onto glass and silicon substrates. The deposited films were fully characterized in terms of chemical composition, crystalline structure, surface morphology, optical and electrical properties. Finally, we investigate the effect of an annealing step at 300° C under argon.

2. Experimental details

2.1. Thin films deposition

Confocal RF magnetron co-sputtering system with angle from the normal of the substrate of 25° (Fig. 1) is used at room temperature to prepare pure and Al-doped ZnO films simultaneously on glass and silicon substrates. The 2-inch circular sources with thickness of 6 mm consisted of ZnO ceramic and aluminum (Al) metal targets with 99.998% and 99.98 % purity, respectively. For a homogeneous film deposition, the samples (25 x 17 mm^2) were placed on a rotating holder in the center of the chamber at a constant rotation

speed of 10 rpm and distance from the target of 80 mm. The importance of using a rotating substrate is to ensure a uniform atom deposition over the whole sample surface. Prior to deposition, glass substrates were first cleaned with acetone and methanol in an ultrasonic bath, then rinsed with distilled water and finally dried in flowing dry nitrogen. Thanks to the load lock chamber, the residual pressure in the deposition chamber was kept at a high vacuum with a base pressure of about 9 x 10^{-6} Pa. Thus, all the films were deposited without breaking vacuum in the deposition chamber under the following conditions: a working pressure of 0.5 Pa using 20 sccm of pure argon (Ar), the RF sputtering power applied to the ZnO target was fixed at 200 W, and the RF sputtering power for the Al target was varying from 0 (undoped film) to 30 W. The deposition time was adjusted between 7 and 10 min to obtain an average thickness of the films of 100 nm. The average deposition rate is estimated at 11 nm/min. Each target was pre-sputtered using a shutter placed between the target and the substrate for 5 minutes at 200 W and 5 Pa with 40 sccm of pure argon prior the beginning of each deposition process. Post-deposition annealing was performed at 300 °C for 1 hour in the deposition chamber under a controlled atmosphere of 10 Pa using 100 sccm of pure Ar.

2.2. Film characterization methods

Several characterization techniques were used to investigate different properties. The chemical composition was achieved by energy dispersive X-ray spectrometry (EDS) using a JEOL 5800 LV Scanning Electron Microscope at 10 kV. The analysis of the surface chemical composition and the bonding states of Zn, Al, and O element were carried out by X-ray photoelectron spectroscopy (XPS) using a Kratos Nova photoelectron spectrometer equipped with a monochromatic Al-K source. The analysis were performed before and after an Ar ion gun sputtering during 60 s at a fixed energy of 0.5 kV, allowing thus a smooth and controlled surface etching, while identifying components related to

contaminations. Casa XPS software was used to fit the high-resolution core-level spectra (Copyright © 2022 Casa Software Ltd, version 2.3.25). The structure and crystalline quality of the deposited films were examined by a grazing incidence X-ray diffraction (GIXRD) with a Thermo-Fisher Inel Equinox 1000 diffractometer at an incidence angle of 2°. Diffraction patterns were recorded using Co-Kα1 radiation (λ=1.789010 Å) in Ω-2θ mode. Surface roughness was analyzed using a Nanosurf Flex Force Microscope (AFM) scan head in contact mode. The images were processed using the free software Gwyddion [48]. The electrical properties (resistivity, ρ, Hall mobility, μ, and carrier concentration, *n*) of as-deposited and annealed films were determined by Hall effect measurements using the Ecopia HMS-5000 system at an applied magnetic field of 0.55 T. A safas UVmc^2 UV-Vis-NIR spectrophotometer was used to record the optical transmission spectra in the 200-1100 nm wavelength range. The optical band gap energy was extracted from the transmission data. Photoluminescence (PL) of the films was examined at room temperature using a Shimadzu RF-6000 spectrofluorophotometer with an excitation wavelength of 350 nm.

3. Results and discussion

3.1. Chemical properties

EDS and XPS analysis were used to determine the bulk and surface chemical composition of the deposited samples, respectively. In order to only quantify the oxygen within the deposited layer, EDS measurements were performed for films deposited on a silicon substrate. The analysis revealed that only Zn, O, Al, and Si elements were detected in the film. On the one hand, the elemental concentrations of Zn, O, and Al vary with the applied power to the Al target. On the other hand, the detected Si signal was assigned to the substrate. To check any variation in Zn, O and Al content, five measurements were taken for each sample. The atomic percentage of each detected element was obtained with a slight deviation of ~0.5%, indicating a uniform distribution of Al in the films.

High resolution XPS spectra of Zn $2p_{3/2}$, Al 2p and O 1s peaks were recorded to analyse the surface chemical composition of pure ZnO and Al-doped ZnO films deposited on glass substrates. All high resolution spectra were calibrated using the carbon C 1s peak position of 284.7 eV and fitted using a Shirley-type baseline for background and a pseudo-Voigt function for each component. Fig. 2 shows the high resolution spectra for the Zn $2p_{3/2}$, Al 2p and O 1s levels after 60 s soft etching. The core level lines of Zn $2p_{3/2}$ and Al 2p appear highly symmetric for all as-deposited films. It also appears that the intensity of the Zn $2p_{3/2}$ peak decreases slowly, whereas the intensity of the Al 2p peak increases with increasing power on the aluminum target from 0 to 30 W. The Zn $2p_{3/2}$ peaks are all located at 1022 ± 0.1 eV without any significant shift with the Al power increase from 0 to 30 W, indicating that the Zn^{2+} valence state associated to ZnO is stable. The Al 2p peak can be fitted by a single Gaussian fit, which means that only one chemical environment is detected of the Al in the doped films. As can be seen in Fig. 2, in the case of pure ZnO film (Bottom blue line), no signal was recorded in the Al 2p region. The Al 2p peak for all doped films is located at 74±0.1 eV, associated to the Al^{3+} valence in the deposited films. Whereas, the high energy resolution O1s peak is asymmetric and can be split into two distinct peaks, labelled O_I and O_{II}, with Gauss-Lorentzian shapes centered at 530.1 ± 0.1 and 531.7 ± 0.1 eV, respectively. The O_I peak at lower binding energy is associated to Zn-O bonds in the wurtzite structure. The O_{II} peak at higher binding energy is attributed to carbonaceous chemisorbed species on the surface of the ZnO films [47]. In fact, this component is reduced by the 60 s Ar ions sputtering, which means that such species are located at the surface of the films and thus associated to surface contaminations.

The Zn, Al, and O atomic contents were calculated using the core levels areas recorded after the etching step (especially for the O 1s level where a component related to surface contamination has been identified and not considered in the calculation). Thus, the

chemical compositions determined by XPS do not include the carbonaceous contamination located at the very surface. Fig. 3 shows the evolution of elemental Zinc, Oxygen and Aluminum contents calculated from the XPS and EDS spectra as a function of the applied power to the aluminum target. As the Al power increases from 0 W (for the undoped film) to 30 W, the Al content increases from 0 to 14 at.% as illustrated by XPS while the Zn content decreased from 52 % to 34 at.%. A similar variation was observed by EDS measurements: the Al content increases from 0 to 11 at. % while the Zn concentration decreases from 50 to 42 at.%. These opposite behaviors between Al and Zn contents were detected by both XPS and EDS measurements. They are indicative of Al atoms incorporation into the ZnO matrix of doped films. However, we have found that the variations of both Al and Zn contents are linear only for the low power values. Indeed, at low Al power (10 W), Al doping of ZnO films can lead to a one-to-one substitution of the Zn atom by Al in the ZnO lattice. Whereas, the Al content in the films deposited at 15 and 20 W deviates slightly from a linear variation. We therefore assume that Al atoms start to occupy both interstitial sites and Zn atoms sites [49]. However, at high Al target power (30 W), Al incorporation seems to reach a saturation level and not only occupy interstitial sites, but also segregate at grain boundaries and lead to distortion of the crystal structure, as shown in the following section. No significant change in the elemental atomic contents was observed between the as-deposited films and the annealed films under a controlled argon atmosphere, indicating that the chemical composition remains stable during the annealing step.

3.2. Structural properties

The GIXRD patterns of the as-deposited and annealed films deposited at various Al target powers (0 to 30 W) are shown in Fig.4. It can be seen, that all thin films are polycrystalline exhibiting the hexagonal Wurtzite structure [50]. All samples show a high (002) diffraction

peak compared to the other diffraction peaks and this is even more pronounced for pure ZnO and the films deposited at low Al power (10 and 15 W), i.e. for lower Al content in the films. At 20 and 30 W deposition power, the intensity of the (002) peak became weaker and broader, which is significant for smaller crystallite sizes and lower crystalline quality. It is interesting to note that for all doped ZnO thin films, no additional peak corresponding to aluminum or any other phase was observed in the GIXRD patterns. The absence of a diffraction peak associated to metallic Al indicates incorporation of Al atoms within the ZnO lattice. This result is in good agreement with observations of I. Valenti et al [51], who obtained a pure wurtzite ZnO matrix without any additional phase for Al content below 14 at. %

The average crystallite size and lattice parameters were determined by the Rietveld refinement method using MAUD software [52]. Rietveld refinements of GIXRD patterns were performed using initial parameters from the zincite structural model (ICDD PDF# 04-016-6648 card). It should be noted that the XRD signal intensity of the film deposited at 30 W is very weak and therefore difficult to be refined. Thus, only the XRD patterns of the films deposited at aluminum target powers ranging from 0 to 20 W were treated. The average crystallite size and d-spacing value versus Al-target power are plotted in Fig.5. The average crystallites size decreases with increasing the Al content in the films. This is believed to be due to ionic size mismatch between Zn^{2+} and Al^{3+} ions and size variation during substitution of Zn^{2+} by Al^{3+} ions at tetrahedral sites. Zhang et al. [53] have observed a grain size decrease and deterioration of film crystallinity as the power is increased on the Al_2O_3 target. Our results are in good agreement with their work. The d-spacing value (right axis in Fig. 5) of the pure ZnO is compatible with the reference value of 2.604 Å given in the ICDD PDF# 04-016-6648 card. In addition, for the film deposited at 10 W, we noticed a shift of the most intense peak (002) to a higher diffraction angle. Such a shift of the

diffraction peak to higher 2θ values indicates a reduction in the lattice spacing distance "d", which obeys to the Bragg's law. This can be attributed to the replacement of Zn^{2+} ions (radius of 0.74 Å) by a smaller Al^{3+} atom (0.54 Å) in the ZnO matrix as reported by Deng et al [54]. Moreover, we also observed a slight shift of the (002) peak position to smaller angle values with increasing Al power from 10 to 20 W, i.e. Al dopant level increase in the films. The corresponding d-spacing parameter increases from 2.61 to 2.65 Å for the films deposited at 10 and 20W, respectively. This increasing trend of the parameter indicates that the ZnO lattice expands along the c-axis as Al atoms are incorporated into the matrix and replace the Zn^{2+} sites as well as occupy the interstitial sites, causing a lattice strain and consequently an increase in the lattice parameter. In addition, for the film deposited at 20 W, there is a large reduction in the (002) peak intensity associated with a significant reduction in the average crystallite size by a factor of 2 from 28 to 13 nm. Furthermore, for the film deposited at 30 W, it is found that the intensities of the XRD pattern diffraction peaks decrease considerably and are significant for a poorer crystalline quality (the reason why the cell parameters and crystallite size were not determined for this sample).

After annealing, the two Bragg diffraction peaks assigned to (002) and (103) planes of a wurtzite structure were clearly observed. Hernandez-Como et al [55] observed an increase in the intensity of the peak (103) with the deposition temperature from 20 to 100°C. Above 75°C the film becomes more polycrystalline due to the increased contribution of the crystallites with the (103) orientation. Again, no additional peaks associated to secondary phases such as metallic Al or Al_2O_3, were observed after the annealing step. The crystallite size increases with annealing and the d-spacing is closer to the reference distance of 2.604 Å (ICDD PDF# 04-016-6648 card), indicating few defects in the films. The features like wurtzite phase of pure ZnO and Al-doped ZnO thin films with low Al content are thus preserved after annealing.

3.3. Surface morphology

The effect of Al doping on the surface morphology of films was investigated by AFM in contact-mode. Root mean squared roughness values (R_{rms}) were determined as an average while considering three scans to minimize local variations. Fig. 6 shows the surface AFM images of the pure ZnO and the Al-doped ZnO for as-deposited films on glass substrate (left hand side) and those annealed at 300°C (right hand side). As can be clearly seen, the surface roughness strongly depends on the Al sputtering power, i.e. Al at.% incorporated. In fact, the addition of Al modifies the surface topography of films from well-defined spherical grains to a smoother surface and smaller grains. For the as-deposited layers, as the power on the Al target increases from 0 to 30 W, the surface roughness decreases by a factor 3 from 1.47 to 0.52 nm. It should be noted that the maximum R_{rms} value was observed for the undoped ZnO thin films and is attributed to the large crystallite size in the ZnO film. Thus, this average higher grain size illustrated by AFM images is in very good agreement with the XRD analysis. For the films annealed for 1 hour at 300°C under a controlled Ar atmosphere of 10 Pa, the same trend, i.e. R_{rms} decrease from 1.71 to 0.58 nm with increasing Al power, was observed. For all samples, a slight increase of the surface roughness is observed after annealing. In all cases, the presented micrographs closely reflect the structural changes described in the previous section. Pure ZnO films show a rougher surface with larger grains, whereas at high Al concentration the deposited films display poorer crystalline quality and smaller grains (as indicated by lower R_{rms} values) in good agreement with small crystallite sizes (as recorded by XRD).

3.4. Optical properties

3.4.1. UV-Vis-NIR transmission

The optical spectra of pure ZnO and Al-doped ZnO thin films deposited on a glass substrate were obtained using a UV-Vis-NIR spectrophotometer in the 200–1100 nm

wavelength range. A glass substrate with a transmission of 90 % was used as a reference sample. Fig. 7 shows optical transmittance, in the visible range, for all samples before and after annealing at different Al sputtering powers. In the case of as-deposited films, when increasing the Al power i.e. Al content, the average optical transmittance of the films taken in the visible range (380-780 nm) decreased from 74 to 26 %. Deposited films with higher Al content (20 and 30 W) exhibit transmittance average values lower than 50 %. Such evolution when the Zn atoms are substituted by Al could be attributed to the variation of free-carrier concentration [56]. Furthermore, the average optical transmittance of all films is increased by annealing; the maximum value of 85 % in the visible range is obtained for the film deposited with a 15 W RF power on the Al target.

To determine the direct optical band gap (E_g) of the deposited films we used the technique based on the first derivative of transmittance (T), dT/dE, as a function of energy (E) [57]. The obtained results are shown in Fig.8; for as-deposited films, an optical band gap of 3.28 eV is obtained for pure ZnO film and a band gap in the range of 3.473 – 4.026 eV is extracted for Al-doped ZnO films. The E_g of Al-doped ZnO films, larger than that of pure ZnO, is well explained by the Burstein-Moss shift [58]. The broadening of the band gap could be due to an increase in the introduced Al impurity density in ZnO lattice. Hence, the present results are in good agreement with those of Liu and Zhang [59] who reported that the band gap widens with increasing Al concentration in Al-doped ZnO thin films synthesized by sol-gel process. Furthermore, for all annealed films, an increase of the band gap values is observed. For the undoped ZnO sample, the band gap increases up to 3.351. Whereas, it increases up to 3.668, 3.746, 3.936 and 4.039 eV for films deposited with increasing Al target power of 10, 15, 20 and 30W, respectively. The highest variation (+ 5.6 %) is obtained for the film with the lower Al content (Al power of 10W). This increase in E_g for the annealed films can be attributed to morphological changes and variations in

carrier concentration. In a previous work [47], we have already observed such a band gap broadening after annealing of AZO films prepared by RF magnetron sputtering of a single target.

3.4.2. Photoluminescence

Photoluminescence (PL) spectroscopy is a powerful technique to obtain information on energy band structure and crystalline quality. For the ZnO structure, PL provides useful information on structural defects such as oxygen vacancies (V_o), zinc vacancies (V_{Zn}), oxygen interstitials (O_i), zinc interstitials (Zn_i) and oxygen anti-sites (O_{Zn}). In this work, room temperature photoluminescence was recorded to study the effects of Al content on the optical response of the deposited films. The obtained results are shown in Fig.9 with the variation of room temperature PL spectra recorded at wavelength of 350 nm for undoped and Al-doped ZnO thin films, as-deposited and after annealing at 300 °C. As can be seen, the PL spectra show a first intense and relatively sharp UV emission centered at 387 nm (3.20 eV) and a second weak blue emission at 469 nm (2.64 eV). The former is attributed to the near-band edge emission (NBE) while the latter is assigned to the singly ionized zinc vacancy V_{Zn}^{+} [60]. The comparison between different spectra led to the following conclusions: (*i*) the annealing process enhances the PL emission for all samples; (*ii*) the highest PL emission is observed for the films deposited at 10 and 15 W, after annealing 1 hour at 300 °C and (*iii*) the lowest PL emission is obtained for the AZO film with the highest Al content in the series, i.e. deposited at a 30 W radio frequency power.

Therefore, it can be observed that the intensity of the UV emission increases with the increasing Al target power up to 15 W for both as-deposited and annealed films, and then decreases for higher power values to reach a minimum emission at 30 W. This PL evolution agrees well with the crystalline quality evolution reported in section 3.2. Therefore, the UV-PL emission seems to depend mainly on the crystalline quality. The

enhancement of UV emission is attributed to the improvement in crystalline quality of ZnO films after annealing. A similar behavior was reported by Xu et al. [61]. However, the decrease in UV emission is probably related to the deterioration of ZnO crystalline quality and the appearance of defects within the structure at high Al content. This degraded crystalline quality is associated to the formation of a high density of grain boundaries and dislocations in the Al-doped ZnO films, resulting in a larger number of non-radiative recombination sites, reducing thus both UV and visible emissions [62].

3.5. Electrical properties

In order to gain some insights in the relationship between the Al content and the electrical properties of the film, the resistivity, carrier concentration and carrier mobility were measured by Hall measurement using the Van der Pauw method. Figure 10 gathers the Hall measurement results for as-deposited (upper part) and annealed films (bottom part) deposited with various Al target RF powers. Hall measurements showed an n-type semiconductor for all studied films. As shown in Fig.10 for the as-deposited films, the carrier concentration increases from 1.66 x 10^{20} cm^{-3} to 22.4 x 10^{20} cm^{-3} as the Al target power is increased from 0 to 30 W. This behavior is in good agreement with the enhancement of bandgap due to impurity density increase as mentioned in section 3.4.1. Moreover, the carrier mobility first increases from 0.69 to 2.52 cm^2/Vs when the Al power is increased from 0 to 15 W and then falls to a value of 0.07 cm^2/Vs for the film deposited at a high Al power of 30 W. It is well known that resistivity is proportional to the reciprocal product of carrier concentration and carrier mobility. In addition, as shown in Fig. 10 for as-deposited films with increasing Al power in the range 0 to 30 W, the resistivity initially decreases to a minimum value of 2.14×10^3 Ω.cm at 15 W and then increases again for the higher Al contents. It can also be noticed that the resistivity of films with low Al content (power in the 10 to 20 W range) is 10 times lower than that of pure

ZnO film. As previously reported, incorporating Al into a ZnO matrix results in an Al-doped ZnO film with a lower resistivity than a pure ZnO film. However, such optimization is limited to a low Al content. A similar trend was previously observed for the resistivity evolution with Al content ranging from 0 to 14 at.% [51]. This is why in our study, doped ZnO films with higher Al content (Al RF power of 30 W) are characterized by a significantly increased resistivity that we associate to the weakening of the structural properties generated by the high doping level. After annealing, under a controlled argon atmosphere at 300 °C for 1 hour, the resistivity of all films is improved and shows a similar trend to the one observed before the heating treatment. A lower resistivity value of 1.55×10^{-3} Ω.cm is obtained for the Al-doped ZnO film deposited at 15 W Al target power after annealing.

3.6. Figure of merit

To evaluate the performance of our undoped and Al-doped ZnO thin films for optoelectronic applications we calculated the figure of merit (FOM) via the most used equation $\boldsymbol{\Phi_{TC} = T^{10}/R_s}$ according to Haacke's work [63], where $\boldsymbol{R_s}$ is the sheet resistance and $\boldsymbol{T}$ is the average optical transmittance of the films in the 400-800 nm range. TCO films with better quality or performance should have the highest FOM value as they represent the best combination of high electrical conductivity and high transmittance in the visible range. Fig. 11 displays the variation of the FOM for the undoped and Al-doped ZnO thin films before and after annealing as a function of Al target RF power. The FOM first increases from 2.3×10^{-4} sq.Ω^{-1} to its maximum value of 43.6×10^{-4} sq.Ω^{-1} for films deposited at 0 and 15 W, respectively, and then decreases to 0.007×10^{-4} sq.Ω^{-1} for the film deposited with the higher Al power of 30 W. After annealing, the same trend is observed for the whole series. In all cases, the annealing process leads to an improvement of the FOM factor by at least one order of magnitude. Interestingly, we found that Al-doped ZnO

thin films deposited at 15 W with an Al content of 3.6 at.% exhibited the best optoelectronic properties since, especially after annealing, the highest FOM value of 43.6 × 10^{-4} sq.Ω^{-1} is obtained. This value is higher than the figure of merit of AZO thin films deposited from a single (ZnO doped 2 wt% Al_2O_3) target reported by Rezaie et al [64] for the film of the same thickness film without an ITO buffer layer and Jun and Koh [65] for the film using the near infrared ray annealing technique. Other works prefer to use a different definition of FOM proposed by Madan et al [66], because the literature does not always report the thickness of the films for which the resistivity was measured. In this case, the equation that are used is ($-1/(\rho \ln T)$) where ρ is the resistivity of the film in Ω.cm and T is the is the average optical transmittance in the visible region 400 to 800 nrn. Also in this case, the figure of merit of ~ 4200 $\Omega^{-1}.cm^{-1}$ obtained on the film deposited at 15W after annealing is much better if compared with the results (~3000) reported by [55] on the films deposited at lower substrate temperature of 20-60°C range. This result is thus optimized compared to the maximum of FOM (34×10^{-4} sq.Ω^{-1}) obtained with AZO film deposited at 50W from a single AZO target (ZnO doped with 2 wt.% of Al_2O_3) and annealed at 400 °C in the same chamber. In addition, this process allows to decrease the thermal budget by lowering the annealing temperature from 400 to 300 °C.

4. Conclusions

ZnO thin films with various Aluminum content in the 0-10 % range were deposited on both glass and silicon substrates by confocal RF magnetron co-sputtering of two Al and ZnO targets. The effect of Aluminum content on the thin films properties was widely investigated. Al content up to 11 (14) at.% range, as determined from EDS (XPS) analysis, was obtained by increasing the power applied to the Al target up to 30 W for a fixed 200 W power on the ZnO target. XRD analysis revealed a hexagonal wurtzite crystalline

structure with a preferential (002) orientation for all deposited films. ZnO films with lower Al atomic content (below 5 % at.) exhibit the best crystalline quality that declines for higher Al content. This result and the opposite variations of Al and Zn contents stand as a proof of Al incorporation into the ZnO network of the doped films. These results are in good agreement with electrical measurements that highlighted a lower resistivity value for Al content in the 5% at. range. All deposited and annealed films presented a relatively low roughness with R_{rms} close to 1 nm. As deposited films exhibit average transmittance, varying from 74 to 26 % in the visible range at room temperature as the Al content is increasing. Annealing allows increasing the optical transmittance for all films and a high transmittance of 85% is achieved for AZO film with Al content of 3.6 at. %. According to the Burstein-Moss effect, the optical band gap values of Al-doped ZnO films are found to increase with the Al content and further increase after annealing at 300 °C. All samples display an intense and sharp UV emission and a very weak blue band in PL analysis. For all films, the UV emission is enhanced after the annealing step at 300 °C under argon. The highest PL intensity was recorded for the film with Al content of 3.6 at. %. Hence, the highest figure of merit (43.6×10^{-4} sq.Ω^{-1}) was obtained for the same AZO film after the annealing step.

This work highlights that by confocal co-sputtering of ZnO and Al targets, the control of RF power applied to the Al target allows to manage finely the Al content in the AZO films. Compared to our previous results obtained with an AZO composite target (Al content of 2 at.%) [45], the FOM is increased from 34×10^{-4} sq.Ω^{-1} to 43.6×10^{-4} sq.Ω^{-1}, by an increase Al content up to 3.6 at.%, *i.e* less than a factor 2. The crucial role of Al content for tuning the structural, optical and electrical properties of Al-doped ZnO thin films is here clearly illustrated.

Homage

The authors want to indicate that at the time of submitting this manuscript, Thierry Chauveau passed away suddenly on July 19th, 2022. Thierry Chauveau was a research engineer at the laboratory of process and materials sciences of the Sorbonne Paris Nord University since 1986. In this work, he participated to XRD measurements and interpretation. This article is entirely dedicated to Thierry Chauveau. The corresponding author, F. Challali is also extremely grateful to him for the many and fruitful scientific discussions they have shared together throughout this collaborative work.

References

[1] K. Ellmer, A. Klein, B. Rech, Transparent Conductive Zinc Oxide Basics and Applications in Thin Film Solar Cells, Springer, (2008).

[2] T. Minami, Transparent conducting oxide semiconductors for transparent electrodes, Semicond. Sci. Technol. 20 (2005) S35–S44. https://doi:10.1088/0268-1242/20/4/004

[3] A. F. Kohan, G. Ceder, D. Morgan, C.G. Van de Walle, First-principles study of native point defects in ZnO, Phys. Rev. B, 61 (2000) 15019-15027. https://doi.org/10.1103/PhysRevB.61.15019

[4] T. Minami, S. Suzuki, T. Miyata, Electrical Conduction Mechanism of Highly Transparent and Conductive ZnO Thin Films. MRS Online Proceedings Library 666, 13 (2000). https://doi.org/10.1557/PROC-666-F1.3

[5] D.V. Vu, D.H. Le, C.X. Nguyen, T.Q. Trinh. Comparison of structural and electric properties of ZnO-based n-type thin films with different dopants for thermoelectric applications. J. sol-gel Sci. Technol. 91 (2019)146–153. https://doi.org/10.1007/s10971-019-05024-0

[6] B.G. Sohany, A.K. Zak, Doped ZnO nanostructures with selected elements - Structural, morphology and optical properties: A review, Ceram. Int. 46 (2020) 5507-5520. https://doi.org/10.1016/j.ceramint.2019.11.051

[7] A. Mallick, D. Basak, Revisiting the electrical and optical transmission properties of co-doped ZnO thin films as n-type TCOs, Prog. Mater. Sci. 96 (2018) 86-110. https://doi.org/10.1016/j.pmatsci.2018.03.004

[8] T. Minami, H. Sato, H. Nanto, S. Takata, Group III Impurity Doped Zinc Oxide Thin Films Prepared by RF Magnetron Sputtering, Jpn. J. Appl. Phys. 24(10A) (1985) L781. https://doi.org/10.1143/JJAP.24.L781

[9] I.Y. Kim, S.W. Shin, M.G. Gang, S.H. Lee, K.V. Gurav, P.S. Patil, J.H. Yun, J.Y. Lee, J.H. Kim, Comparative study of quaternary Mg and Group III element co-doped ZnO thin films with transparent conductive characteristics, Thin Solid Films, 570 (2014) 321-325. https://doi.org/10.1016/j.tsf.2014.02.109

[10] J. Liu, W. Zhang, D. Song, Q. Ma, L. Zhang, H. Zhang, X. Ma, H. Song, Comparative study of the sintering process and thin film sputtering of AZO, GZO and AGZO ceramics targets, Ceram. Int. 40 (8B) (2014) 12905-12915. https://doi.org/10.1016/j.ceramint.2014.04.150.

[11] D.S.Y. Jayathilake, Jagdeep S. Sagu, K. G. U. Wijayantha , Transparent heater based on Al,Ga co-doped ZnO thin films, Mater. Lett. 237 (2019) 249-252. https://doi.org/10.1016/j.matlet.2018.11.092

[12] J. Liu, W. Zhang, D. Song, Q. Ma, L. Zhang, H. Zhang, X. Ma, H. Song, Comparative study of the sintering process and thin film sputtering of AZO, GZO and AGZO ceramics targets, Ceram. Int., 40 (2014) 12905-12915. https://doi.org/10.1016/j.ceramint.2014.04.150

[13] Y.M. Hu, J.Y. Li, N.Y. Chen, C.Y. Chen, T.C. Han, C.C. Yu, Effect of sputtering power on crystallinity, intrinsic defects, and optical and electrical properties of Al-doped ZnO transparent conducting thin films for optoelectronic devices, J. Appl. Phys., 121 (2017) 085302. https://doi.org/10.1063/1.4977104

[14] M. Lee, Y. Park, K. Kim, J. Hong, Influence of sputtering conditions on the properties of aluminum-doped zinc oxide thin film fabricated using a facing target sputtering system, Thin Solid Films, 703 (2020) 137980. https://doi.org/10.1016/j.tsf.2020.137980.

[15] M. Mickan, U. Helmersson, D. Horwat, Effect of substrate temperature on the deposition of Al-doped ZnO thin films using high power impulse magnetron sputtering, Surf. Coat. Technol. 347 (2018) 245-251. https://doi.org/10.1016/j.surfcoat.2018.04.089.

[16] D.S.Y. Jayathilake, Jagdeep S. Sagu, K.G.U. Wijayantha, Transparent heater based on Al,Ga co-doped ZnO thin films, Mater. Lett. 237 (2019) 249-252. https://doi.org/10.1016/j.matlet.2018.11.092.

[17] H. Rotella, Y. Mazel, S. Brochen, A. Valla, A. Pautrat, C. Licitra, N. Rochat, C. Sabbione, G. Rodriguez, E. Nolot, Role of vacancy defects in Al doped ZnO thin films for optoelectronic devices. J. Phys. D: Appl. Phys. 50 (2017) 485106. https://doi.org/10.1088/1361-6463/aa920b

[18] K. Remashan, Y. S. Choi, S. J. Park, J. H. Jang, Impact of near-stoichiometric silicon nitride gate insulator on the performance of MOCVD-grown ZnO thin-film transistors, ECS J. Solid State Sci. Technol., 1 (4) (2012) 70-78. http://dx.doi.org/10.1149/2.006204jss

[29] S. D. Ponja, S. Sathasivam, I. P. Parkin, C. J. Carmalt. Highly conductive and transparent gallium doped zinc oxide thin films via chemical vapor deposition. Sci Rep 10, (2020) 638. https://doi.org/10.1038/s41598-020-57532-7

[20] A. Omerzu, R. Peter, D. Jardas, I. Turel, K. Salamon, M. Podlogar, D. Vengust, I. J. Badovinac, I. K. Piltaver, M. Petravic, Large enhancement of photocatalytic activity in

ZnO thin films grown by plasma-enhanced atomic layer deposition, Surf. Interfaces, 23 (2021) 100984. https://doi.org/10.1016/j.surfin.2021.100984.

[21] K. Necib, T. Touam, A. Chelouche, L. Ouarez, D. Djouadi, and B. Boudine, Investigation of the effects of thickness on physical properties of AZO sol-gel films for photonic device applications, J. Alloys Compd. 735 (2018) 2236–2246. https://doi.org/10.1016/j.jallcom.2017.11.361.

[22] N. Srinatha, P. Raghu, H. M. Mahesh, B. Angadi, Spin-coated Al-doped ZnO thin films for optical applications: Structural, micro-structural, optical and luminescence studies, J. Alloys Compd. 722 (2017) pp. 888-895. https://doi.org/10.1016/j.jallcom.2017.06.182.

[23] G. Kaur, A. Mitra, K. Yadav, Pulsed laser deposited Al-doped ZnO thin films for optical applications. Prog. Nat. Sci.: Mater. Int., 25 (2015) 12-21. https://doi.org/10.1016/j.pnsc.2015.01.012

[24] Y. Aoun, B. Benhaoua, S. Benramache, B. Gasmi, Effect of deposition rate on the structural, optical and electrical properties of zinc oxide (ZnO) thin films prepared by spray pyrolysis technique, Optik, 126 (2015) 2481-2484. https://doi.org/10.1016/j.ijleo.2015.06.025

[25] K. Matsubara, P. Fons, K. Iwata, A. Yamada, K. Sakurai, H. Tampo, S. Niki, ZnO transparent conducting films deposited by pulsed laser deposition for solar cell applications, Thin Solid Films, 431–432 (2003) 369-372. https://doi.org/10.1016/S0040-6090(03)00243-8

[26] H. Makino, H. Shimizu, Influence of crystallographic polarity on the opto-electrical properties of polycrystalline ZnO thin films deposited by magnetron sputtering, Appl. Surf. Sci. 439 (2018) 839-844. https://doi.org/10.1016/j.apsusc.2018.01.107

[27] Hongyan Liu, Xiaoqiang Wang, Mingya Li, Shujin Yu, Rongxu Zheng, Optical and electrical properties of Al doped ZnO thin film with preferred orientation in situ grown at room temperature, Ceramics International 45 (2019) 14347-14353. https://doi.org/10.1016/j.ceramint.2019.04.149

[28] B.C. Bussell, P.N. Gibson, J. Lawton, P. Couture, M.K. Sharpe, J. England, S.J. Hinder, V. Stolojan, S.A. Thornley, M.A. Baker, The effect of RF plasma power on remote plasma sputtered AZO thin films, Surface and Coatings Technology, 442 (2022) 128402. https://doi.org/10.1016/j.surfcoat.2022.128402

[29] Rajan Singh & S. K. Mukherjee, Correlation of structural, electrical and optical properties of Al-doped ZnO TCOs, Journal of Materials Science: Materials in Electronics, 33, (2022) 6969–6980. https://doi.org/10.1007/s10854-022-07876-9

[30] Long Wen, Manish Kumar, B.B. Sahu, S.B. Jin, C. Sawangrat, K. Leksakul, J.G. Han, Advantage of dual-confined plasmas over conventional and facing-target plasmas for improving transparent-conductive properties in Al doped ZnO thin films, Surface and Coatings Technology, 284 (2015) 85-89. https://doi.org/10.1016/j.surfcoat.2015.06.084

[31] Luo Chen and Xiaofang Bi, Variations of microstructure, conductivity and transparency of Al-doped ZnO thin films prepared by radio frequency magnetron sputtering with target–substrate distances, Vacuum 82 (2008) 1216-1219. https://doi.org/10.1016/j.vacuum.2008.02.008

[32] Martin Mickan, Ulf Helmersson, David Horwat,Effect of substrate temperature on the deposition of Al-doped ZnO thin films using high power impulse magnetron sputtering,

Surface and Coatings Technology 347 (2018) 245-251. https://doi.org/10.1016/j.surfcoat.2018.04.089

[33] J. Rezek, P. Novák, J. Houška, A.D. Pajdarová, T. Kozák, High-rate reactive high-power impulse magnetron sputtering of transparent conductive Al-doped ZnO thin films prepared at ambient temperature Thin Solid Films 679 (2019) 35-41, https://doi.org/10.1016/j.tsf.2019.04.009

[34] I.H Kim, D.Y. Ku, J.H. Ko, D. Kim, K.S. Lee, J.H. Jeong, T.S. Lee, B. Cheong, Y.J. Baik, W.M. Kim, Improvement of the thermal and chemical stability of Al doped ZnO films. J Electroceram 17, 241–245 (2006). https://doi.org/10.1007/s10832-006-8315-8

[35] R. E Treharne, K Hutchings, D. A Lamb, S .J.C Irvine, D Lane and K Durose, Combinatorial optimization of Al-doped ZnO films for thin-film photovoltaics, Journal of Physics D: Applied Physics 45 (2012) 335102 10.1088/0022-3727/45/33/335102

[36] Xue-Yong Li, Hong-Jian Li, Zhi-Jun Wang, Hui Xia, Zhi-Yong Xiong, Jun-Xi Wang, Bing-Chu Yang, Effect of substrate temperature on the structural and optical properties of ZnO and Al-doped ZnO thin films prepared by dc magnetron sputtering, Optics Communications, 282 (2009) 247-252. https://doi.org/10.1016/j.optmat.2018.06.024

[37] Joondong Kim, Ju-Hyung Yun, Sang-Won Jee, Yun Chang Park, Minkyu Ju, Seokkyu Han, Youngkuk Kim, Jae-Hyun Kim, Wayne A. Anderson, Jung-Ho Lee, Junsin Yi, Rapid thermal annealed Al-doped ZnO film for a UV detector, Materials Letters, 65 (2011) 786-789. https://doi.org/10.1016/j.matlet.2010.11.065

[38] Li-Yu Lin, M. Chang Jeong, Dae-Eun Kim, Jae-Min Myoung Micro/nanomechanical properties of aluminum-doped zinc oxide films prepared by radio frequency magnetron sputtering, Surface and Coatings Technology 201 (2006) 2547-2552. https://doi.org/10.1016/j.surfcoat.2006.04.067

[39] Yu-Yun Chen, Jin-Cherng Hsu, Chun-Yi Lee & Paul W. Wang Influence of oxygen partial pressure on structural, electrical, and optical properties of Al-doped ZnO film prepared by the ion beam co-sputtering method, Journal of Materials Science volume 48, pages 1225–1230 (2013). https://doi.org/10.1007/s10853-012-6863-7

[40] Lirong Sun, John T. Grant, John G. Jones, Neil R. Murphy, Tailoring electrical and optical properties of Al-doped ZnO thin films grown at room temperature by reactive magnetron co-sputtering: From band gap to near infrared, Optical Materials, 84(2018) 146-157. https://doi.org/10.1016/j.optmat.2018.06.024

[41] M. Jullien, D. Horwat, F. Manzeh, R. Escobar Galindo, Ph. Bauer, J.F. Pierson, J.L. Endrino, Influence of the nanoscale structural features on the properties and electronic structure of Al-doped ZnO thin films: An X-ray absorption study Solar Energy Materials & Solar Cells 95 (2011) 2341–2346. https://doi.org/10.1016/j.solmat.2011.04.003

[42] Eugen Stamate, "Spatially Resolved Optoelectronic Properties of Al-Doped Zinc Oxide Thin Films Deposited by Radio-Frequency Magnetron Plasma Sputtering Without Substrate Heating, Nanomaterials 2020, 10, 14; doi:10.3390/nano10010014

[43] Kion Norrman, Poul Norby and Eugen Stamate, "Preferential zinc sputtering during the growth of aluminum doped zinc oxide thin films by radio frequency magnetron sputtering" J. Mater. Chem. C, 2022, 10, 14444–14452, DOI: 10.1039/d2tc02180c

[44] Beyza T¨onbül, Hilal Aybike Can, Tayfur ¨Oztürk, Hasan Akyıldız, "Solution processed aluminum-doped ZnO thin films for transparent heater applications", Materials Science in Semiconductor Processing 127 (2021) 105735, https://doi.org/10.1016/j.mssp.2021.105735

[45] F.C. Correia, P.B. Salvador, J.M. Ribeiro, A. Mendes, C.J. Tavares, "Effect on the electrical and morphological properties of Bi incorporation into ZnO:Ga and ZnO:Al thin

films deposited by confocal magnetron sputtering" Vacuum 152 (2018) 252-260 https://doi.org/10.1016/j.vacuum.2018.03.033

[46] R E Treharne, K Hutchings, D A Lamb, S J C Irvine, D Lane and K Durose, "Combinatorial optimization of Al-doped ZnO films for thin-film photovoltaics", J. Phys. D: Appl. Phys. 45 335102, http://dx.doi.org/10.1088/0022-3727/45/33/335102

[47] F. Challali, D. Mendil, T. Touam, T Chauveau, V. Bockelée, A-G Sanchez, A. Chelouche, M-P Besland, Effect of RF sputtering power and vacuum annealing on the properties of AZO thin films prepared from ceramic target in confocal configuration, Mater. Sci. Semicond. Proc. 118 (2020) 105217

https://doi.org/10.1016/j.mssp.2020.105217

[48] D. Nečas, P. Klapetek, Gwyddion: open-source software for SPM data analysis, Cent. Eur. J. Phys. 10 (2012) 181–188.https://doi.org/10.2478/s11534-011-0096-2.

[49] S. Mandal, H. Mullick, S. Majumdar, A. Dhar, S. K. Ray, Effect of Al concentration in grain and grain boundary region of Al-doped ZnO films: a dielectric approach, J. Phys. D: Appl. Phys. 41 (2008) 025307. https://iopscience.iop.org/article/10.1088/0022-3727/41/2/025307

[50] M. J. Zhao, Z. T. Sun, C. H. Hsu, P. H. Huang, X. Y Zhang, W. Y. Wu, P. Gao, Y. Qiu, S.-Y. Lien, W. Z. Zhu. Zinc Oxide Films with High Transparency and Crystallinity Prepared by a Low Temperature Spatial Atomic Layer Deposition Process. Nanomater.10(3) (2020) 459. https://doi.org/10.3390/nano10030459

[51] I. Valenti, S. Benedetti, A. di Bona, V. Lollobrigida, A. Perucchi, P. Di Pietro, S. Lupi, S. Valeri, and P. Torelli, Electrical, optical, and electronic properties of Al:ZnO films in a wide doping range, J. Appl. Phys. 118, (2015) 165304. https://doi: 10.1063/1.4934512

[52] L. Lutterotti, S. Matthies, H. Wenk, MAUD: a friendly Java program for material analysis using diffraction, CPD Newsletter 21 (1999) 14–15. http://hdl.handle.net/11572/38076

[53] Ming Zhang, Yankun Tang, Xin Tian, Hairong Wang, Jiuhong Wang, Qunming Zhang, Magnetron co-sputtering optimized aluminum-doped zinc oxide (AZO) film for high-response formaldehyde sensing, Journal of Alloys and Compounds 880 (2021) 160510. https://doi.org/10.1016/j.jallcom.2021.160510

[54] Z. Deng, C. Huang, J. Huang, M. Wang, H. He, H. Wang, Y. Cao, Effects of Al content on the properties of ZnO:Al films prepared by Al_2O_3 and ZnO co-sputtering, J. Mater. Sci: Mater. Electron. 21 (2010) 1030–1035. https://doi.org/10.1007/s10854-010-0084-0

[55] N. Hernandez-Como, A. Morales-Acevedo, M. Aleman, I.Mejia, M.A. Quevedo-Lopez, " Al-doped ZnO thin films deposited by confocal sputtering as electrodes in ZnO-based thin-film transistors" Microelectronic Engineering 150 (2016) 26–31 http://dx.doi.org/10.1016/j.mee.2015.10.017

[56] T. Dimopoulos, G. Z. Radnoczi, Z. E. Horváth, H. Brückl, Increased thermal stability of Al-doped ZnO-based transparent conducting electrodes employing ultra-thin Au and Cu layers, Thin Solid Films 520 (2012) 5222–5226. https://doi.org/10. 1016/j.tsf.2012.03.103

[57] T. Touam, M. Atoui, I. Hadjoub, A. Chelouche, B. Boudine, A. Fischer, A. Boudrioua, A. Doghmane, Effects of dip-coating speed and annealing temperature on structural, morphological and optical properties of sol-gel nano-structured TiO2 thin films, Eur. Phys. J. Appl. Phys. 67 (2014) 30302. https://doi.org/10.1051/epjap/2014140228.

[58] S. H. Jeong, D. -G. Yoo, D. Y. Kim, N.-E. Lee, J. -H. Boo, Physical properties and etching characteristics of metal (Al, Ag, Li) doped ZnO films grown by RF magnetron

sputtering, Thin Solid Films, 516 (19) (2008) 6598-6603. https://doi.org/10.1016/j.tsf.2007.11.034.

[59] W. L. Liu and Y. F. Zhang, Blue shift of absorption edge and photoluminescence in Al doped ZnO thin films, Integr. Ferroelectr. 188 (2018) 112–120, https://doi.org/10.1080/10584587.2018.1454222

[60] A. Chelouche, T. Touam, K. Necib, L. Ouarez, F. Challali, D. Djouadi , Investigation of the effects of drying process on microstructural and luminescence properties of Al-doped ZnO thin films, J. Lumin. 219 (2020) 116891. https://doi.org/10.1016/j.jlumin.2019.116891

[61] L. Xu, X. Li, Y. Chen, F. Xu, Structural and optical properties of ZnO thin films prepared by sol–gel method with different thickness, Appl. Surf. Sci. 257 (2011) 4031–4037. https://doi.org/10.1016/j.apsusc.2010.11.170

[62] J. B. You, X.W. Zhang, Y.M. Fan, Z.G. Yin, P.F. Cai, N.F. Chen, Effects of crystalline quality on the ultraviolet emission and electrical properties of the ZnO films deposited by magnetron sputtering, Appl. Surf. Sci. 255 (2009) 5876–5880, https://doi.org/10.1016/j.apsusc.2009.01.024

[63] G. Haacke, New figure of merit for transparent conductors, J. Appl. Phys. 47 (1976) 4086–4089. https://doi.org/10.1063/1.323240

[64] M.N. Rezai, N. Manavizadeh, E. Nadimi, F.A. Boroumand, Quality enhancement of AZO thin films at various thicknesses by introducing ITO buffer layer. J Mater Sci: Mater Electron 28, 9328–9337 (2017). https://doi.org/10.1007/s10854-017-6671-6

[65] M-C. Jun and J-H Koh, "Effects of NIR annealing on the characteristics of al-doped ZnO thin films prepared by RF sputtering" Nanoscale Res Lett. 2012; 7(1): 294. doi: 10.1186/1556-276X-7-294

[66] R.E.I. Schropp and A. Madan, "Properties of conductive zinc oxide films for transparent electrode applications prepared by rf magnetron sputtering" Journal of Applied Physics 66, 2027 (1989); doi: 10.1063/1.344341. http://dx.doi.org/10.1063/1.344341

Figures captions

Fig.1. Schematic of the experimental co-sputtering configuration and image of the plasma during the process in insert.

Fig.2. XPS core level spectra of Zn $2p_{3/2}$, Al 2p and O 1s recorded after 60 s soft etching of ZnO thin films deposited on glass substrates versus Al target power from 0 to 30 W.

Fig.3. Atomic contents of zinc, aluminum, and oxygen extracted from XPS and EDS analysis for films deposited on glass and silicon substrates, respectively and versus RF power on the Al target.

Fig.4. Grazing incidence XRD patterns of undoped and Al-doped ZnO thin films prepared at room temperature on glass substrates for different Al target sputtering powers before and after 1 hour in situ annealing at 300°C under Ar pressure. Experimental patterns are shown with a black open diamond and the Rietveld refinement result is given by a solid colored line.

Fig.5. Average crystallite size and atomic d-spacing of as-deposited and annealed Al-doped ZnO films prepared on a glass substrate as function of the Al target sputtering power

Fig.6. Semi-2D AFM images of undoped and Al-doped ZnO thin films deposited on a glass substrate as a function of Al target power before and after annealing at 300°C.

Fig.7. Optical transmittance spectra of undoped and Al-doped ZnO thin films deposited on glass substrates at different Al RF sputtering powers (a) as-deposited and (b) annealed at 300°C

Fig.8. dT/dE curves obtained from transmittance spectra of Al-doped ZnO thin films deposited on glass substrates at different RF sputtering powers before and after annealing at 300°C.

Fig.9. PL spectra of as-deposited and annealed Al-doped ZnO thin films deposited on glass substrates at different Al target sputtering powers

Fig.10. Electrical properties (resistivity, carrier mobility and carrier concentration) obtained by Hall measurement for the as-deposited and annealed Al-doped ZnO thin films as a function of Al RF sputtering power

Fig.11. Figure of merit of deposited films versus Al target sputtering powers before and after annealing at 300°C under controlled argon atmosphere.

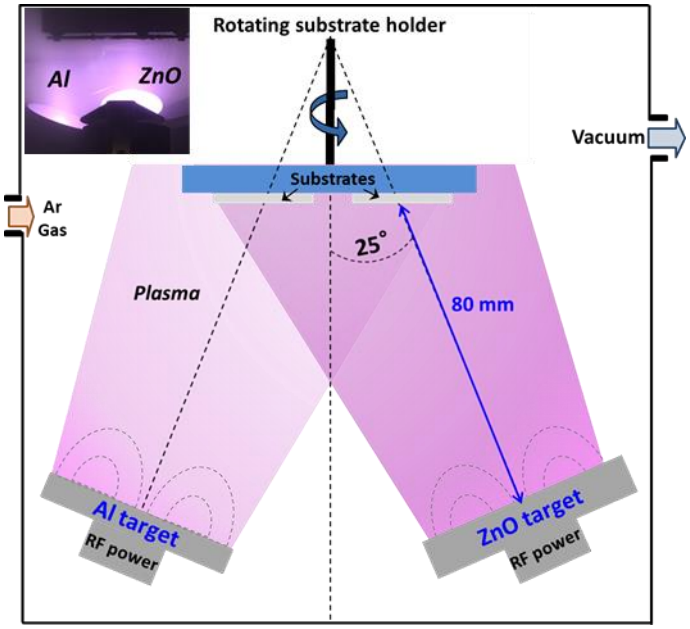
Al
ZnO
Rotating substrate holder
Vacuum
Substrates
Ar
Gas
25°
Plasma
80 mm
Al target
RF power
ZnO target
RF power

Fig.1

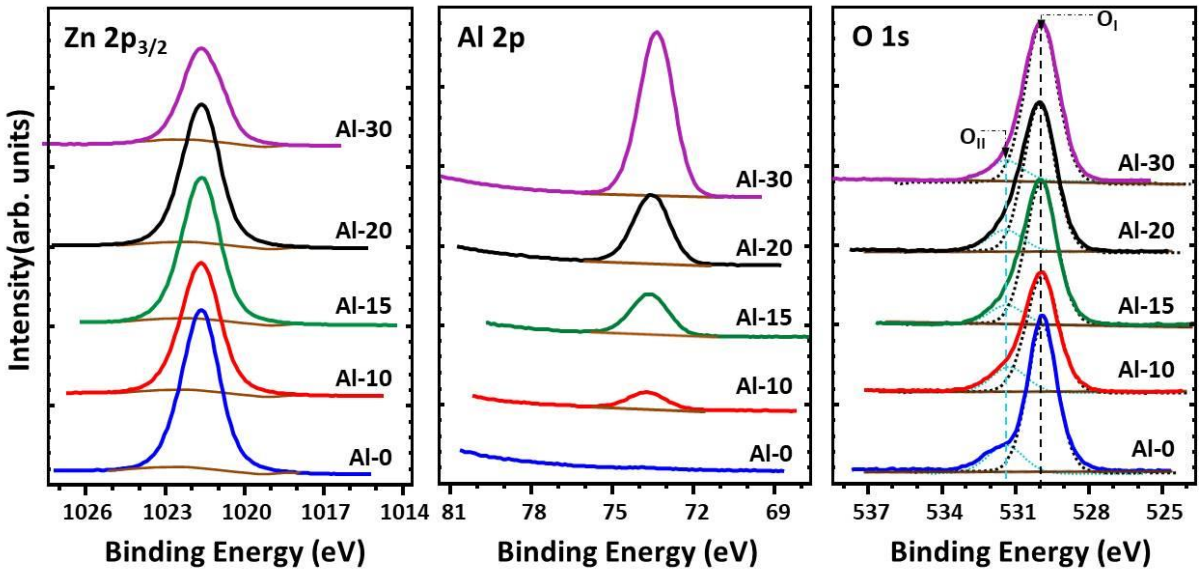
Zn 2p3/2
Al 2p
O 1s
OI
OII
Al-30
Al-20
Al-15
Al-10
Al-0
Intensity(arb. units)
1026 1023 1020 1017 1014
81 78 75 72 69
537 534 531 528 525
Binding Energy (eV)
Binding Energy (eV)
Binding Energy (eV)

Fig.2

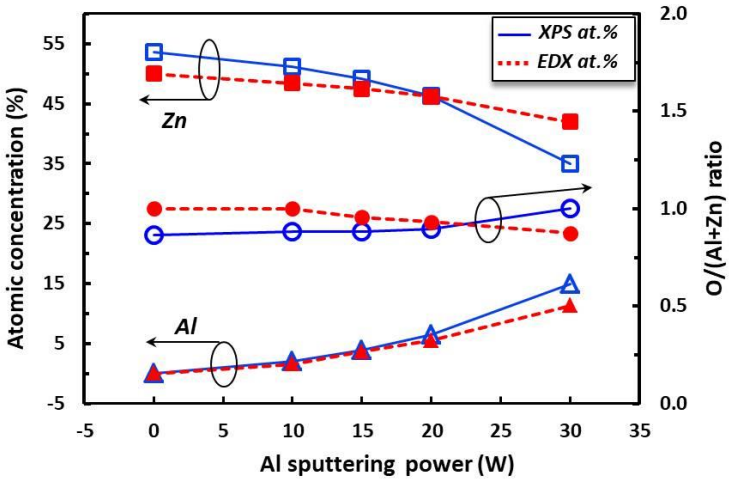
XPS at.%
EDX at.%
Zn
Al
Atomic concentration (%)
O/(Al+Zn) ratio
Al sputtering power (W)
55
45
35
25
15
5
-5
2.0
1.5
1.0
0.5
0.0
-5
0
5
10
15
20
25
30
35

Fig.3

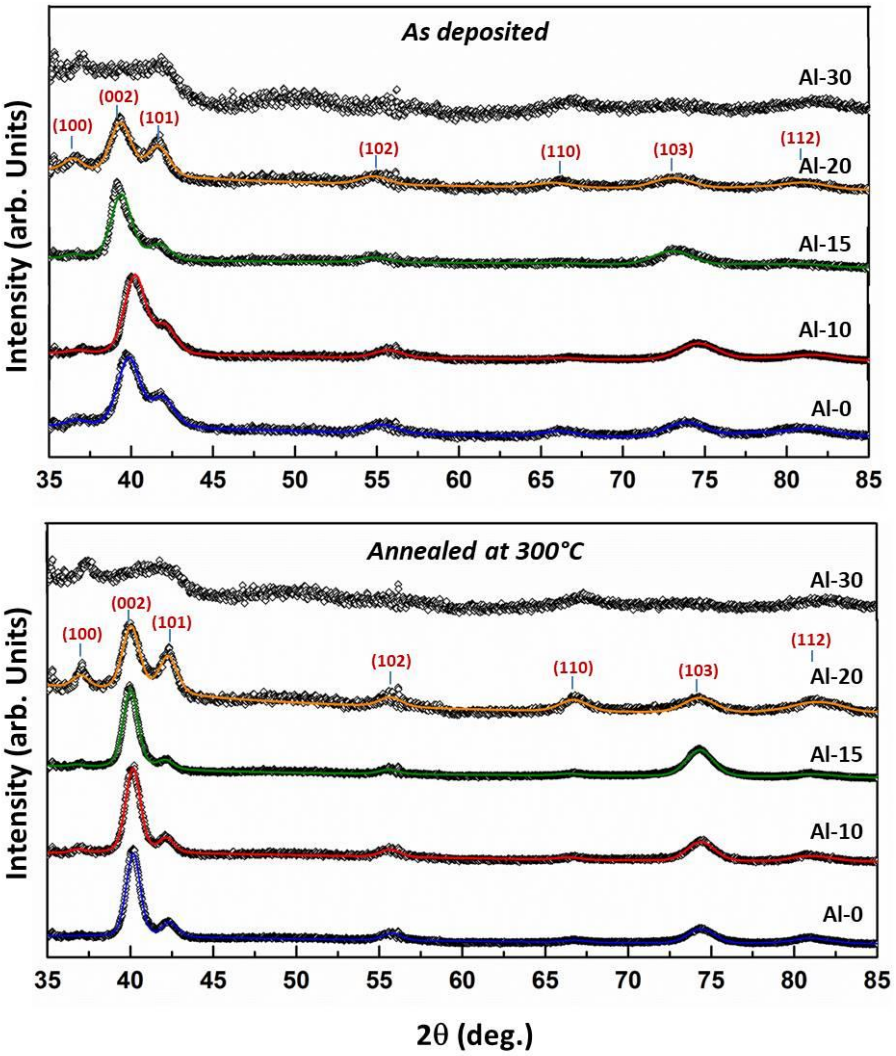
As deposited
Al-30
(002)
(100)
(101)
(102)
(110)
(103)
(112)
Al-20
Al-15
Al-10
Al-0
Intensity (arb. Units)
35
40
45
50
55
60
65
70
75
80
85
Annealed at 300°C
Al-30
(002)
(100)
(101)
(102)
(110)
(103)
(112)
Al-20
Al-15
Al-10
Al-0
Intensity (arb. Units)
35
40
45
50
55
60
65
70
75
80
85
2θ (deg.)

Fig.4

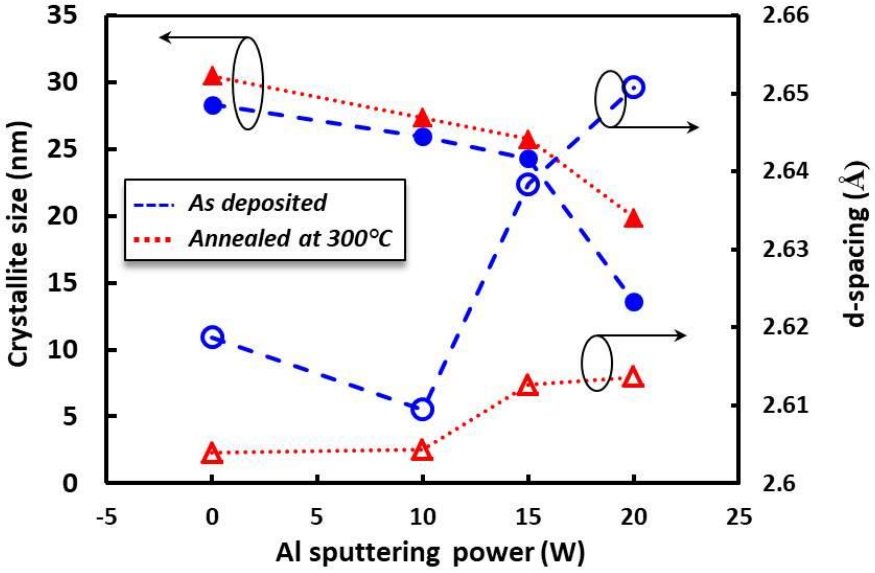
Crystallite size (nm)
d-spacing (Å)
Al sputtering power (W)
As deposited
Annealed at 300°C
35
30
25
20
15
10
5
0
2.66
2.65
2.64
2.63
2.62
2.61
2.6
-5
0
5
10
15
20
25

Fig.5

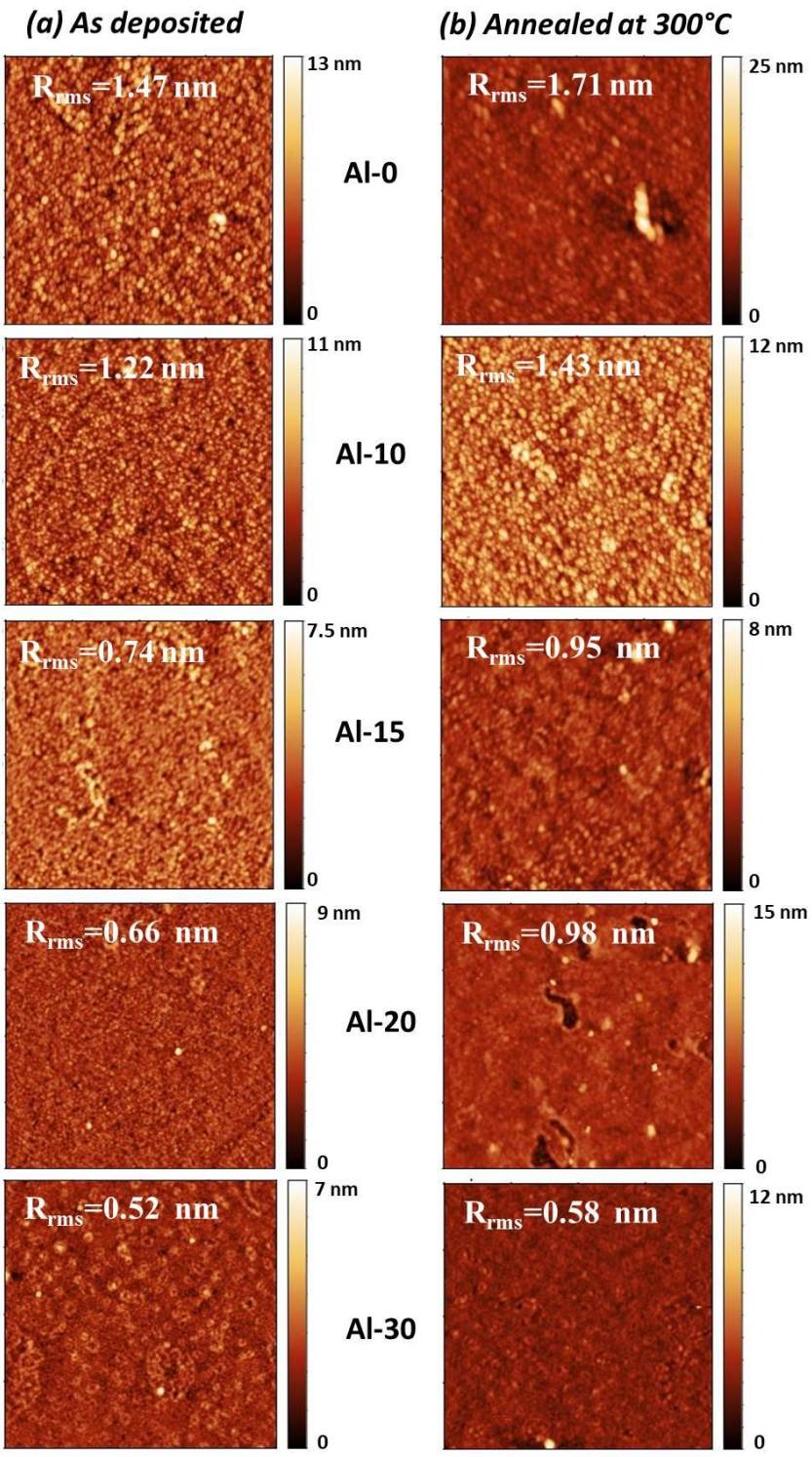
(a) As deposited
(b) Annealed at 300°C
R_rms=1.47 nm
13 nm
0
Al-0
R_rms=1.71 nm
25 nm
0
R_rms=1.22 nm
11 nm
0
Al-10
R_rms=1.43 nm
12 nm
0
R_rms=0.74 nm
7.5 nm
0
Al-15
R_rms=0.95 nm
8 nm
0
R_rms=0.66 nm
9 nm
0
Al-20
R_rms=0.98 nm
15 nm
0
R_rms=0.52 nm
7 nm
0
Al-30
R_rms=0.58 nm
12 nm
0

Fig. 6

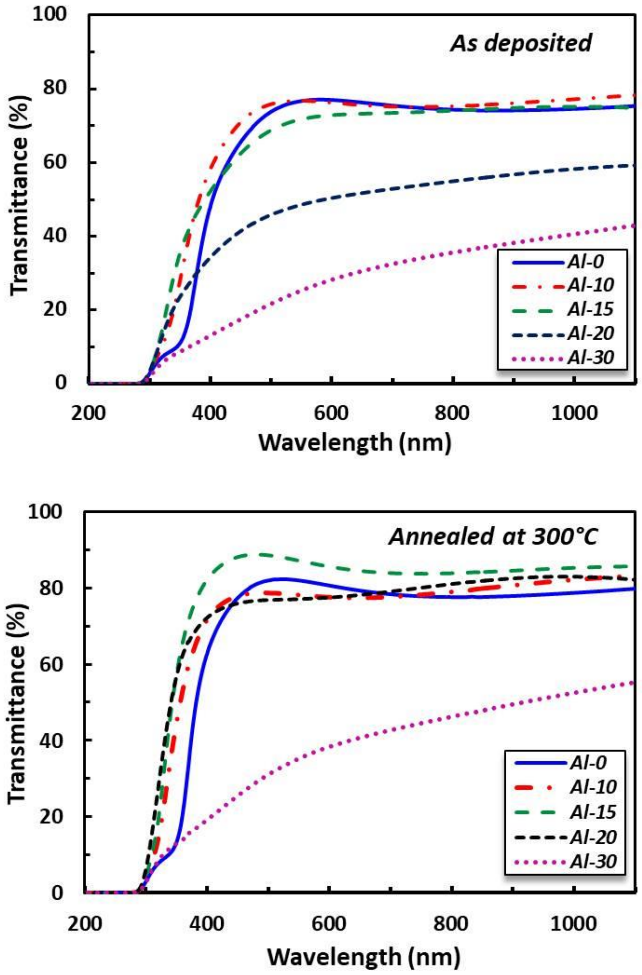
As deposited
Transmittance (%)
Wavelength (nm)
Al-0
Al-10
Al-15
Al-20
Al-30
Annealed at 300°C
Transmittance (%)
Wavelength (nm)
Al-0
Al-10
Al-15
Al-20
Al-30

Fig.7

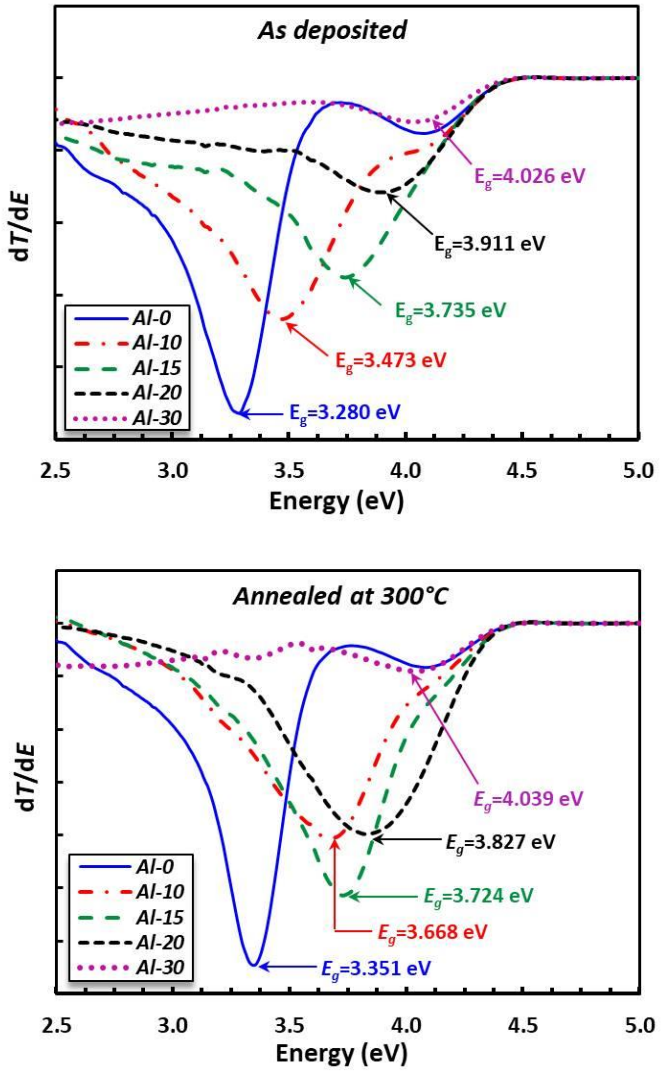
As deposited
dT/dE
Al-0
Al-10
Al-15
Al-20
Al-30
Eg=4.026 eV
Eg=3.911 eV
Eg=3.735 eV
Eg=3.473 eV
Eg=3.280 eV
2.5
3.0
3.5
4.0
4.5
5.0
Energy (eV)
Annealed at 300°C
dT/dE
Al-0
Al-10
Al-15
Al-20
Al-30
Eg=4.039 eV
Eg=3.827 eV
Eg=3.724 eV
Eg=3.668 eV
Eg=3.351 eV
2.5
3.0
3.5
4.0
4.5
5.0
Energy (eV)

Fig.8

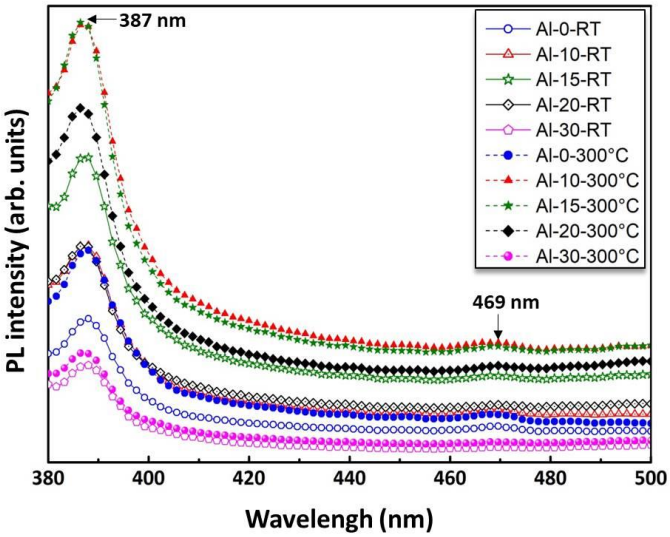
387 nm
469 nm
Al-0-RT
Al-10-RT
Al-15-RT
Al-20-RT
Al-30-RT
Al-0-300°C
Al-10-300°C
Al-15-300°C
Al-20-300°C
Al-30-300°C
PL intensity (arb. units)
Wavelengh (nm)
380
400
420
440
460
480
500

Fig.9

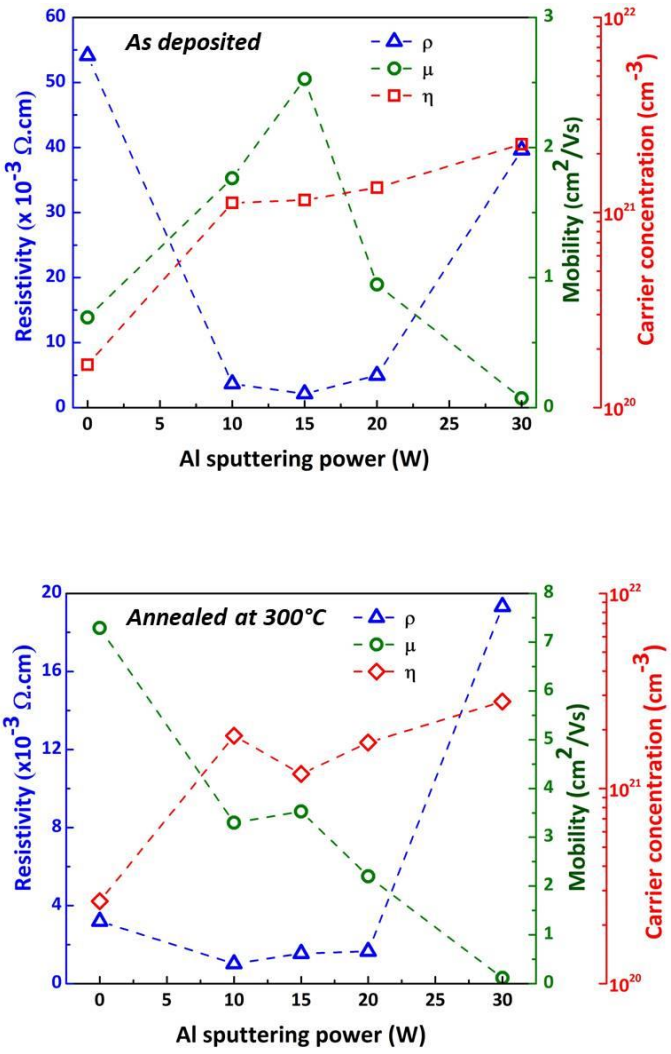
As deposited
ρ
μ
η
Resistivity (x 10^-3 Ω.cm)
Mobility (cm^2/Vs)
Carrier concentration (cm^-3)
Al sputtering power (W)
Annealed at 300°C
ρ
μ
η
Resistivity (x10^-3 Ω.cm)
Mobility (cm^2/Vs)
Carrier concentration (cm^-3)
Al sputtering power (W)

Fig. 10

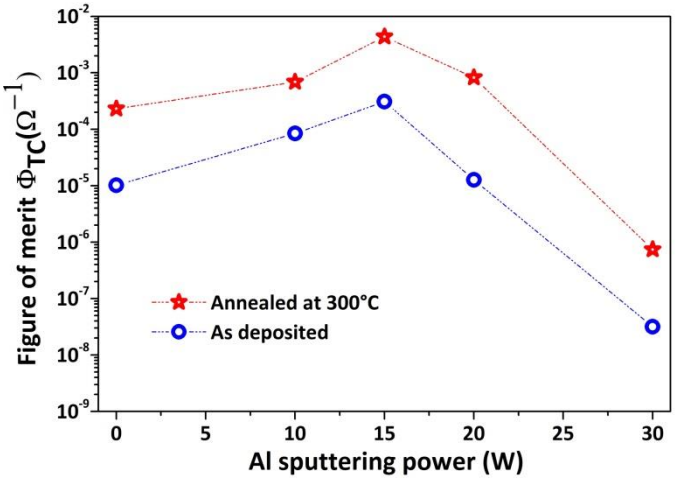
Figure of merit $\Phi_{TC}(\Omega^{-1})$
10^{-2}
10^{-3}
10^{-4}
10^{-5}
10^{-6}
10^{-7}
10^{-8}
10^{-9}
0
5
10
15
20
25
30
Al sputtering power (W)
Annealed at 300°C
As deposited

Fig. 11